Understanding spatial and temporal control of T-cell signaling using designed protein scaffolds and live imaging

Hailemikael Yirdaw

A thesis
submitted in partial fulfillment of the
requirements for the degree of

Master of Science

University of Washington
2024

Committee:
Hao Kueh
Elizabeth Wayne

Program Authorized to Offer Degree:
Bioengineering

University of Washington

Abstract

Understanding spatial and temporal control of T-cell signaling using designed protein scaffolds and live imaging

Hailemikael Yirdaw

Chair of the Supervisory Committee:

Hao Kueh
Department of Bioengineering

T-cells can discriminate between foreign and self-peptides through a process known as kinetic proofreading, where time lag in signaling enables the cell to selectively respond to stably binding foreign peptides. Kinetic proofreading is believed to arise in the T-cell receptor (TCR) signaling pathway; however, the exact biochemical reactions in this pathway that underlie proofreading have remained unclear. A recent experimental modeling study in our lab attributed proofreading to the phosphorylation, diffusion, and condensation of a key signaling protein, LAT, following TCR and peptide major histocompatibility complex (pMHC) binding. This model uses time delays in the nucleation of LAT clusters and condensates for kinetic proofreading, allowing very selective and persistent responses to high-affinity pMHC ligands. Moreover, the nucleation and growth of LAT condensates also amplify low signals from foreign peptides. Our model predicts that LAT condensation and clustering occur optimally at intermediate pMHC densities. Here, to test this key prediction, we used a protein scaffold to present pMHCs at defined intervals and measured resultant signaling through LAT and other associated components through immunofluorescence staining and imaging. We further used live imaging to test the model. Here in these experiments, we cloned reporter proteins for key TCR signaling pathway components both upstream and downstream of LAT (*TCRz, LAT, ZAP70, Grb2, and PLCg*), and transfected them into a Jurkat T-cell line. We then measured phosphorylation and activation responses in T-cells using live imaging. These tools will allow us to test model predictions and broadly investigate the dynamics and mechanisms of antigen discrimination through T-cell signaling.

Introduction

The immune system plays an important role in cancer detection, organ transplants, autoimmune diseases, and vaccine development. Understanding how it works would help to advance medical treatment and vaccine production. The immune system's working mechanism depends extremely on signal transduction pathways and the spatial structure of cell-cell interactions. T-cells play a crucial role in cellular immunity as they recognize antigenic peptides on the surface of MHC-presenting cells[2,3]. T-cell signaling in the immune system includes immunological synapse formation, and phase separation and condensation of signaling components[1, 3, 7]. T-cell signaling can be understood at the molecular level using the nucleation condensation model[1, 3, 15].

In the immune system initiation phase, immune synapse formation is one of the important steps that allows the TCR to effectively communicate with antigen-presenting cells (APC) [3,5,24]. The spatial structure of the immune synapse is crucial for the immune system's ability to recognize and respond to infections. The immunological synapse, a dynamic junction between T cells and antigen-presenting cells (APC), is a key component of T cell signaling[4,5,12,25]. The synapse's architecture, including the peripheral supramolecular activation cluster (pSMAC) and central supramolecular activation cluster (cSMAC), facilitates the effective transmission and amplification of necessary signals[6].T cell receptors and pMHCs are found in the cSMAC, while adhesion molecules like LFA-1 maintain the synapse in the pSMAC[3,6]. The actin cytoskeleton is essential for arranging the spatial distribution of receptors and signaling molecules at the immunological synapse, which is constantly reconfigured[1,7,29].

Phase separation and condensation procedures enhance the development of immunological synapses by causing local concentration variations and promoting molecular interactions [2,11,18,21,26]. This results in dynamic, liquid-like condensates of signaling molecules, improving signal quality and reaction speeds[8,17,30]. Tiny, unstable clusters of signaling molecules first form at the immunological synapse, where they attract additional molecules to evolve into stable forms[2,3,11]. The spatial structure of the synapse, facilitated by membrane microdomains and cytoskeletal rearrangements, ensures proper localization and interaction of signaling molecules, allowing for accurate regulation of T-cell activation and efficient immune responses[8,9,10,31].

The model created in our lab, which is based on the condensation of LAT, demonstrates how the spacing of the pMHC might affect the LAT nucleation and condensation[3]. The spacing of MHC molecules in T-cell activation is well known and understood[4,15]; however, it is limited and has not been utilized to determine the signaling pathways and downstream effects of MHC spacing [3,25]. We currently know a limited amount of information on how spacing affects activation and do not understand well if a specific spacing has been preferred to maximize activation. The work in our lab on arrays revealed that changing spacing affects signaling, revealing an effect and determining the preferred spacing. We hope to fill that gap using this model[3].

Our lab developed a dynamic model to understand the function of LAT condensation in TCR signaling[3]. TCRs and LAT molecules were able to spread freely because the model was constructed on a two-dimensional grid that was meant to resemble a T-cell's plasma membrane[3]. The actions of several molecules, including Grb2, LAT molecules, ZAP70, Lck, PLCγ, SOS, and CD45, on TCRs were used [3].

Using probabilities, the model computes the activities of each molecule separately and modifies the simulation grid accordingly. Not taken into account in previous models, this model addresses signaling effects caused by regional inhomogeneities which leads to clustering. The assumptions made for this model were that using ZAP70, LAT gets phosphorylated immediately when the pMHC binds with TCR. The process was designed to skip certain steps for ease and to confirm that the observed results were solely due to LAT clustering.

The impacts of extra phosphorylation processes are excluded from the study, which concentrates on the function of LAT condensation at the beginning of T-cell signaling[3,5,12]. Four pY sites are phosphorylated by the pMHC-bound TCR at LAT; three of these sites are prime substrates for the kinase ZAP70, while the Y132 site is phosphorylated at a lesser rate[1,3,25]. Since the Y132 site's delayed phosphorylation represents a rate-limiting step at the start of the T-cell signal, it is simulated independently[3]. Two kinds of pLAT are modeled: p3LAT, which lacks phosphorylation on Y132 and can only bind other p3LAT through weaker Grb2-SOS-mediated connections, and p4LAT, which has all pY sites phosphorylated and may engage in PLCγ-mediated bonding[3]. Because of these reversible interactions, LAT's pY sites build a network of linkages that enable it to form a condensate.

Phosphatases work against pLAT condensate formation by dephosphorylating pLAT, which prevents it from cross-linking[3,5,21]. A larger degree of protection was provided by the stronger binding of PLCγ to pY132 than by the weaker Grb2/SOS mediated links[3]. From the model, we were able to observe that the intermediate spacing of pMHC gives better LAT clustering and condensation[3]. This result is supported by experimental data from fixed-cell imaging[3]. Here we validate these concepts using quantitative real-time live imaging techniques, which required cloning and cell line preparation, to track T-cell responses to antigen over time. The methods developed here enable live imaging of T-cell signaling and help validate the computational model.

Chapter 1

Designed protein scaffolds reveal spatial dependencies in T-cell signaling

The T-cell, by interacting with MHC, can selectively recognize the foreign peptides on infected cells, but ignore self-peptides on healthy cells. Many kinetic proofreading models have been established to understand the T-cell and TCR working mechanisms to distinguish self and foreign antigens[9,13]. From these models, we were able to understand that the condensation of LAT was crucial for the activation of downstream signaling and responding to antigens very effectively.

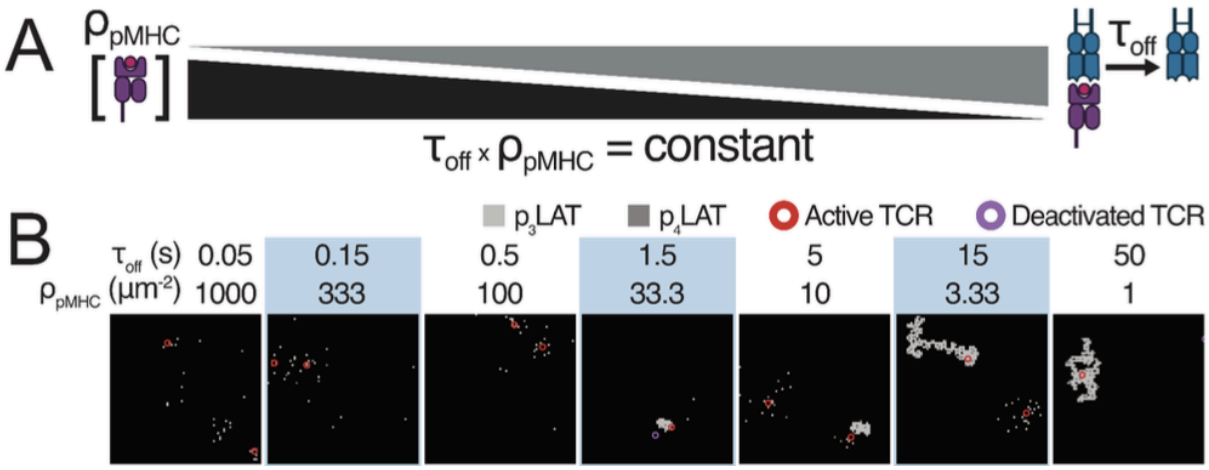

Figure 1: Condensate nucleation provides kinetic proofreading in TCR signaling [3]. *Information from models with pMHC binding lifetimes while maintaining constant TCR occupancy. For every condition, 750 duplicate simulations were performed. A) Diagram illustrating how the number of bound TCRs is maintained by concurrently increasing the pMHC-TCR bond lifetime and decreasing the pMHC 2D density. B) Screenshots of typical simulations using WT LAT at every pMHC off-rate. Gray squares indicate phospho-LAT. Circles show bound TCRs; purple indicates deactivated, and red indicates active. A 2.25-μm square is represented by each figure[3].*

Predictions about pMHC spacing

Our prediction about the pMHC spacing is that the higher density of MHC would lead to higher phosphorylation and activation of TCR and LAT condensation[3]. Our lab examined the relationship between single-molecule imaging investigations and simulations of LAT clustering dynamics. The LAT condensation simulations predict the optimal pMHC spacing for TCR activation. In our lab data from simulations with 16 fixed pMHCs at varying spacings and WT LAT were used. 500 replicate simulations were run for each pMHC density[3].

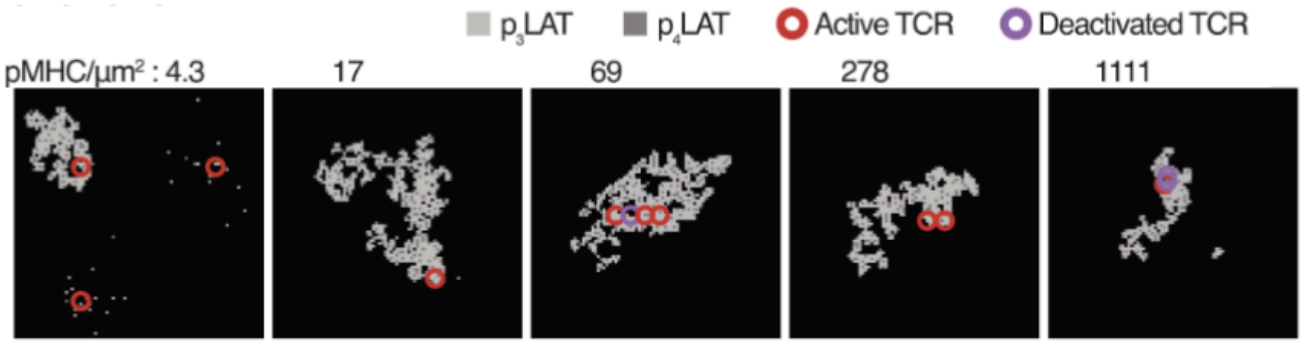

Figure 2: ***This is an example of simulations at different pMHC densities[3]****. Light gray squares symbolize p3LAT, and dark gray squares symbolize p4LAT. Circles symbolize bound TCRs: red for active and purple for deactivated. Each snapshot was distributed in a 1.27-μm square[3].*

The optimal spacing is determined by the underlying cause of optimal spacing[3]. At low pMHC density, pMHC-bound TCRs are isolated, preventing pLAT from forming a condensate at neighboring TCRs. At intermediate pMHC density, pLAT can add to a condensate nucleated at neighboring TCRs. At high

pMHC density, neighboring pMHC-bound TCRs are crowded, limiting the area over which a condensate can form.

Arrays were used to test the impact.

An imaging test was conducted to investigate the relationship between antigen density and LAT clustering, aiming to verify the prediction of ideal pMHC density[3]. We positioned pMHCs at regular intervals on a 2D protein array, consisting of two components: the Component A is fused to SpyCatcher exclusively, while component B is fused to GFP exclusively, and A binds to B.[3,44]. Combining these components results in a hexagonal grid that self-assembles[3]. The activation of the TCR is initiated by the presence of MHC that binds with the array[3].

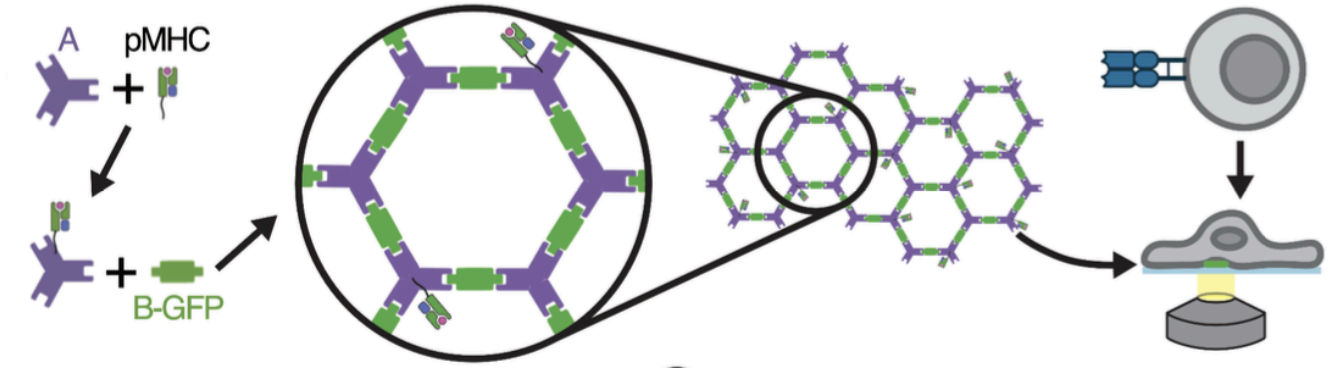

Figure 3*: 2D protein arrays enable precise pMHC display, with components A fused with SpyCatcher and B fused with GFP depicted as purple triangles and green rectangles respectively, and a 31nm distance between opposing hexagonal unit edges[3].*

The 2D density of pMHCs on arrays can be adjusted by changing the stoichiometry of SpyTag-pMHC, and SpyCatcher-A before assembly with component B[3]. We used SpyCatcher because it is a versatile tool that forms a strong, specific, and irreversible covalent bond with SpyTag, ensuring stability under harsh conditions[35]. It is useful for bioconjugation, creating complex assemblies and multifunctional proteins, and enhances protein engineering by facilitating efficient attachment of domains and tags[35]. Random fluctuations in array sizes can be used to evaluate the effects of pMHC spacing and number on TCR signaling[3].

We observed that the array can stimulate cell activation, and we used the GFP component of the array to trace the stimulation. We tested a range of pMHC densities and measured their ability to activate T-cells through the induction of LAT clustering[3]. We tested 8 different spacings of pMHC, where the rations of pMHC and A component were in different densities of pMHC/um^2, including 2400, 1200, 600, 300, 150, 75, and 37.5, and the negative control was 0 pMHC/um^2. Those different concentration ratios show the spacing impact that the pMHC would have on the activation and condensation of LAT, forming a cluster. The MHC binding with component A of the array can be adjusted by altering the ratio between the array and MHC, affecting the spacing and density of pMHC.

From the previous work in our lab, we found that intermediate pMHC spacings show a higher efficiency of LAT clustering and activation[3]. Here in Figure 4, we can see the concentration per micrometer square of the pMHC compared to the average clustering. We revealed that there is an optimal spacing of

pMHC for a better response and activation[3]. In this stimulation, we observed that the intermediate pMHC was preferred, and the experimental results matched the stimulation.

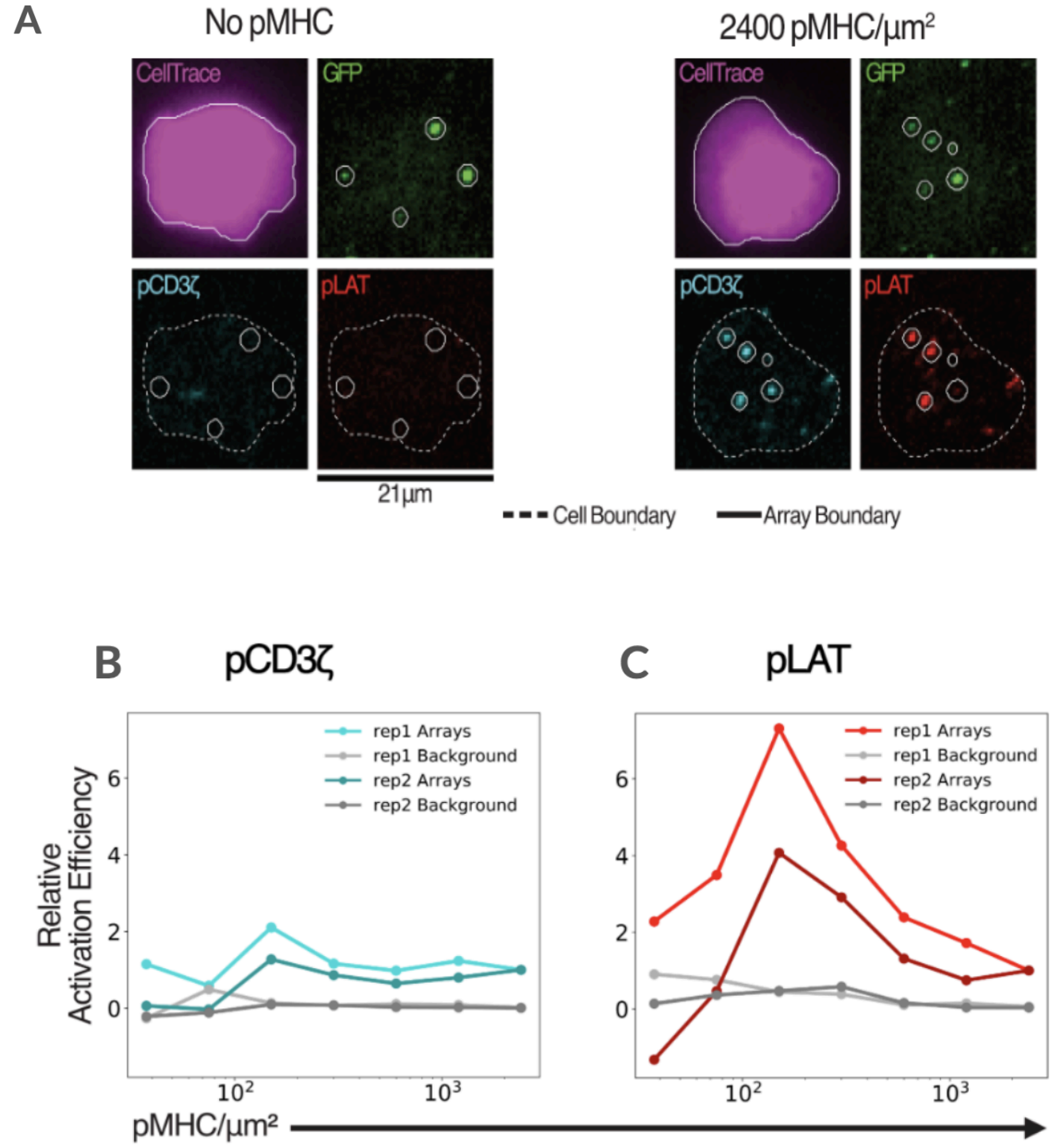

Figure 4: The ideal pMHC spacing for LAT phosphorylation is shown using 2D arrays[3]. *A, Demonstrates that when pMHC is present, pLAT and CD3z are activated, contrasting with no pMHC.In both B and C, line graphs displaying the activation effectiveness of CD3ζ (B)or LAT (C) for arrays (color) or background (gray) as a function of pMHC density. The slope of the line that best fits the connection between overall phosphorylation intensity and pMHC number is known as activation efficiency. The data presented are from two biological replicates (rep1 and rep2), where each replication has been separately standardized to the efficiency at 2400pMHC/µm2 [3].*

Chapter 2

Probing T cell signaling dynamics using live imaging

Chapter one discusses the impact of pMHC spacing on immune system response and LAT cluster formation. The project was motivated by a model developed by Will White in the lab. The previous project focused on fixed cell imaging, which was sufficient to understand signaling cascades and LAT clustering formation. However, to better understand the behavior of LAT clustering and formation during live imaging, we started a project to determine the dynamics of clustering in live cells.

Live-cell imaging techniques can help to understand how spatial proximity affects signaling specificity and efficiency[32]. The single protein tracking approach reveals the movements and interactions of individual proteins within the cell, which is fundamental for understanding mechanisms like signal amplification and kinetic proofreading during T-cell activation[3,7,19,25]. Integrating the computational model we have with live-cell imaging data will lead to a comprehensive understanding of signaling networks and their contribution to cellular signaling. Understanding mechanisms like signal amplification and kinetic proofreading during T-cell activation requires grasping the motions and interactions of specific proteins within the cell[3,6,18,31]. In general, integrating computational models with live-cell imaging data could lead to the understanding of activation and signaling networks and their role in cellular signaling[32].

It is more efficient to use reporter proteins to track the activation and phosphorylation of LAT and CD3z for this project; therefore, we made reporter proteins by creating fusions of signaling proteins with fluorescent proteins. Therefore we found that cloning the reporter and using them was necessary for this project. We made cell lines with reporters for live imaging.

Cloning mRuby and iRFP reporters

The signaling proteins we are interested in are *TCR, LAT, ZAP, Grb2, and PLCg* because these five proteins serve as markers for LAT condensation and T-cell activation. We tagged these proteins with mRuby or iRFP to visualize them by fluorescence microscopy.

We had a set of plasmids when we first began the cloning procedure, which we utilized to construct the plasmid containing the fluorescent protein[34]. Using those initial plasmids, we used fluorescent proteins such as mRuby and iRFP, which excite at different wavelengths in the visible spectrum of light. Fluorescent proteins respond well to specific wavelength lasers during imaging, allowing us to visualize each protein independently.

Using PCR to amplify the specific part of the sequence in each plasmid and insert it with the desired plasmid using Gibson ligation we were able to make the reporters. The fluorescent protein was incorporated into the pLenti plasmids using a Gibson assembly method, as illustrated in Fig 5.

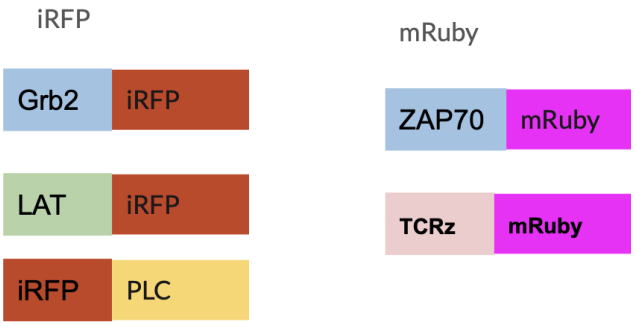

Figure 5: *Schematic diagram of mRuby and iRFP tagging the reporters*

ZAP70 and TCRz were tagged with mRuby fluorescent protein, whereas GRB2, LAT, and PLCg were labeled with iRFP. Our choice of those two fluorescent proteins stems from the fact that their excitation and emission peaks are distinct from GFP, which is attached to the array, and to our anti-CD69 antibody that we will subsequently use to detect the presence or absence of cell activation, as CD69 is correlated with both cell activation and phosphorylation[3,19,21,25].

The reporter cell line is created by combining reporters in pairs.

The reporter pairs were ZAP with PLCg, ZAP with Grb2, and TCRz with LAT. We make sure that the fluorescent protein tags on the two proteins are distinct when we couple them. The other was to make sure they were linked using an intuitive pairing approach, for instance. Grb2, PLCg, and LAT are clustered proteins, while TCR and ZAP are not. Therefore, they were not paired with each other, resulting in one protein in each cluster and one not in the clustering, among other important considerations, it makes more sense to be able to track both aspects of signlaing at the same time.

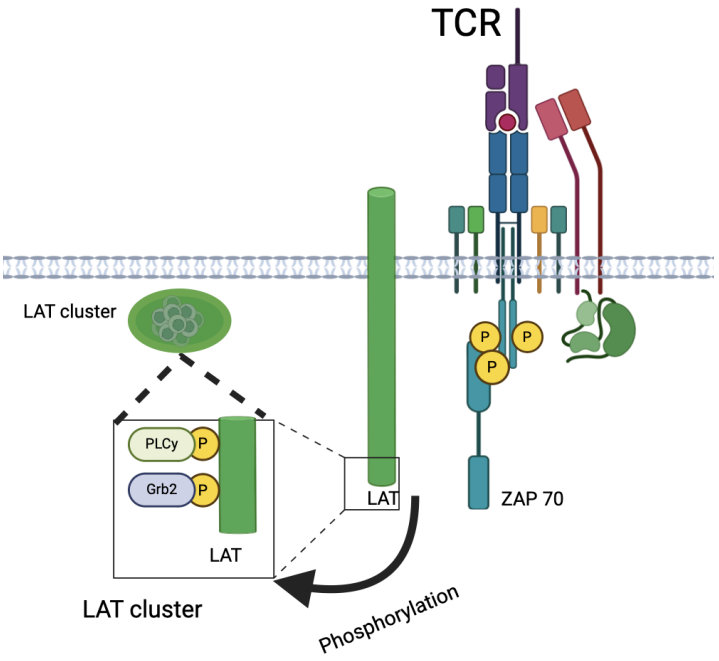

Figure 6: (Left)**Schematic diagram of pair reporter, (Right)** ***Indicates that TCR and ZAP are not clustered, but LAT, PLCg, and Grb2 are.*** *Following Zap-70's phosphorylation, proteins attach to LAT, triggering subsequent immune responses.*

For each reporter pair, we made a cell line. We used HEK cells to produce the lentivirus for each reporter and transfected them into Jurkat cells in pairs. After infecting the Jurkats, we used FACS to sort the cells that expressed both reporter proteins in the pair as shown in Figure 7. These states were further categorized based on cell expression and dividing cells into high and low for each type to determine which cell line would be least affected by the reporters'

presence during activation. We were able to see how diverse the cells were for each reporter and had more cells to choose from by dividing them into low and high groups.

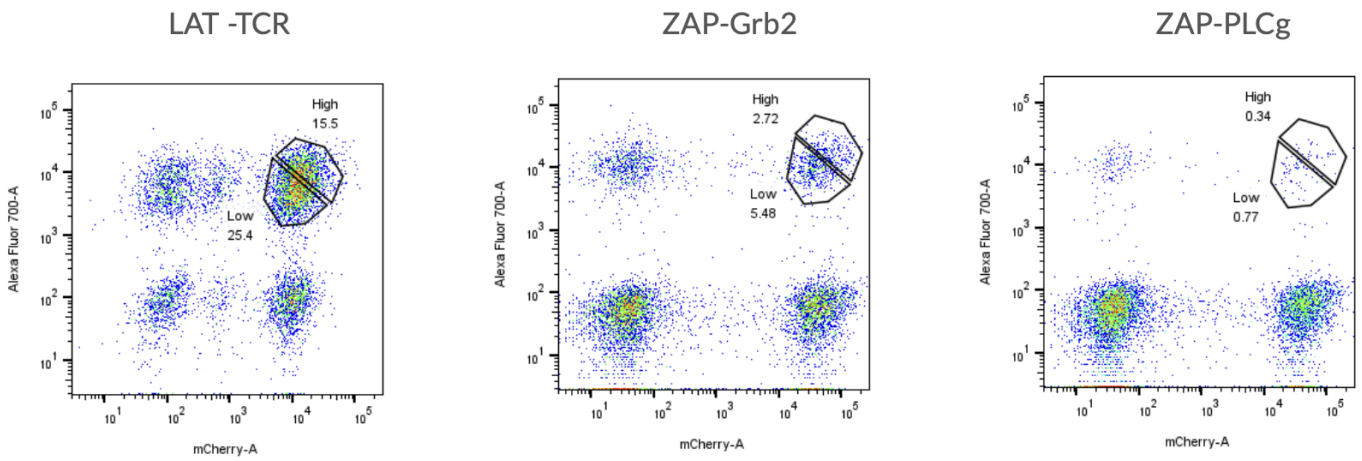

Figure 7: *Here is an example of how we make the gate for high and low for each category.*

By doing the same thing for three of them, we now have high and low reporter populations for each pair of reporters. Using some of the frozen and thawed cells, we ran another experiment to see which of the two cell lines the high and the low would function better in each case. We stimulated the cells with plate-bound anti-CD3/CD28 antibodies and used flow cytometry to measure CD69 expression.

For this experiment, we used a range of anti-CD3/CD28 antibody concentrations, from 6nM to 40 uM, a negative control (0 uM), and a positive control (PMA/ionomycin). We tested each of these conditions with each sorted reporter population and an unmodified cell line as a control.

Here in Figure 8, we aim to observe the differences between the low and high populations for each pair.

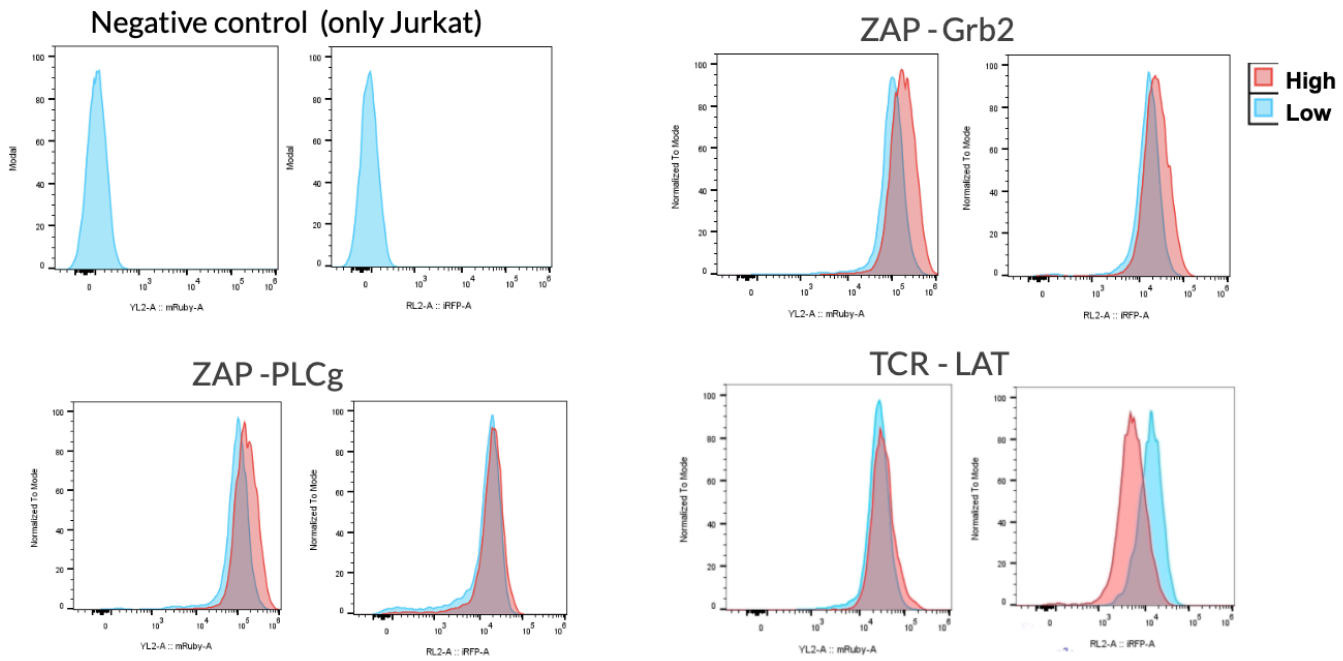

Figure 8: *This demonstrates negative control(only Jurkat) without the reporter proteins. For the other three the presence of mRuby and iRFP in reporter proteins, with high and low curves showing proportions.*

In Figure 8, no significant difference exists between high and low levels, confirming that well-separated low and high levels were small and quite enough to separate them from one another.

As shown in the graph in Figure 8 the high and low show the difference of their iRFP and mRuby for each cell, confirm our sorting was correct and it is visible here, we saw similar graphs for all of those three pairs. However, this does not mean one of them is better than the other in terms of activation.

We aimed to determine the impact of the reporter on the cell's activation. To avoid interference with the activation mechanism, it is essential to avoid any influence. If the reporter were affecting the activation, it would be challenging to tell if it was due to the spacing of MHC or the presence of the reporter activating the T cell. Consequently, we needed to ensure that the reporters did not affect the T-cell's activation. We did an experiment that involved placing a reporter in Jurkat cells to test if activation was affected by the reporters. We used flow cytometry to check the reporter's response, and we concluded that the presence of these reporter proteins did not affect the fluorescence and activation of the cell.

The variation in anti-CD69 concentration reveals a distinct expression of activation on CD69.

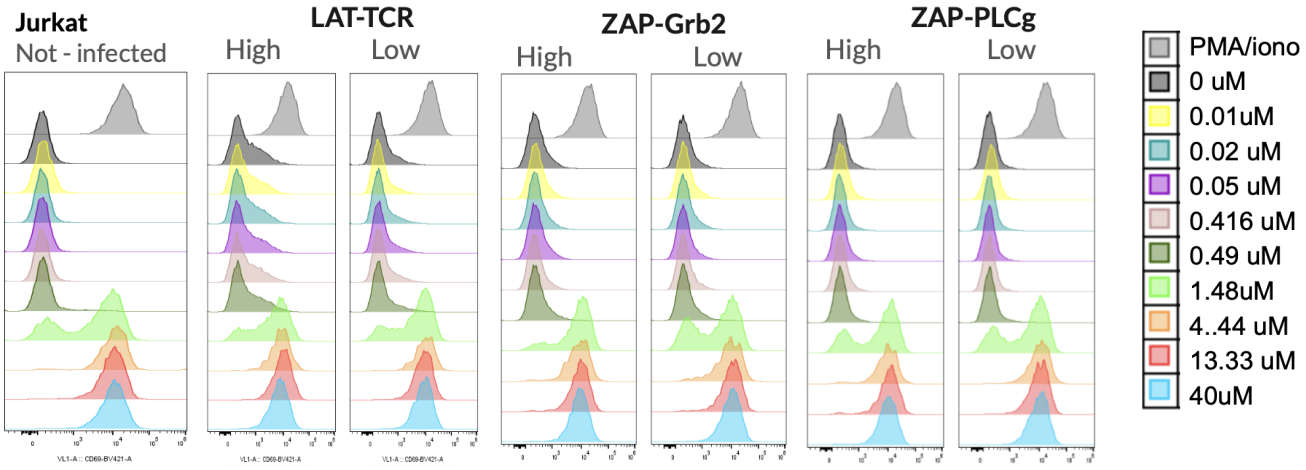

Figure 9: Activation of CD69 with different concentrations of anti-CD3/CD28 antibody and positive and negative controls. *The figure demonstrates the minimal difference between low and high cell types, with each couple responding similarly.*

The variation between conditions shows a yes-or-no response with no middle ground, as each plot is relatively far to the right or left for each unique concentration. Figure 9 shows that there is not much of a difference between low and high kinds of cells. Since each of the three couples responds comparably, we are free to select whatever option we wish. As each plot in Figure 9 has a roughly bimodal distribution for each unique concentration, we can observe that CD69 expression is a yes-or-no response with no middle ground. We also observe that activation is only possible at concentrations of 1.48 uM or higher. Figure 9 plots reveal that the cutoff or threshold is 1.48 uM concentration, and the types of cells in each cell category don't matter.

Live imaging results.

Live imaging shows array spacing varies with concentrations (2400, 1200, 600, 300, 150, 75, and 37.5) and negative control of 0 pMHC/um^2, indicating over-time variation. Eight different spacings were

tracked, demonstrating a similar tracing mechanism for all concentrations, which is used to determine Grb2 expression. We can trace the activation using the presence and frequency of Grb2 because we used the ZAP-Grb2 kind of cell. In Figure 10, the ZAP70 and Grb2 clusters may be observed as brighter patches where they have gathered. As seen in Fig. 9, the development of those clusters demonstrates the phosphorylation of ZAP, which results in the formation of LAT clustering. Grb2 and PLCg are also connected to and present in the LAT cluster. As a result, the Grb2 cluster's formation indicates LAT clustering.

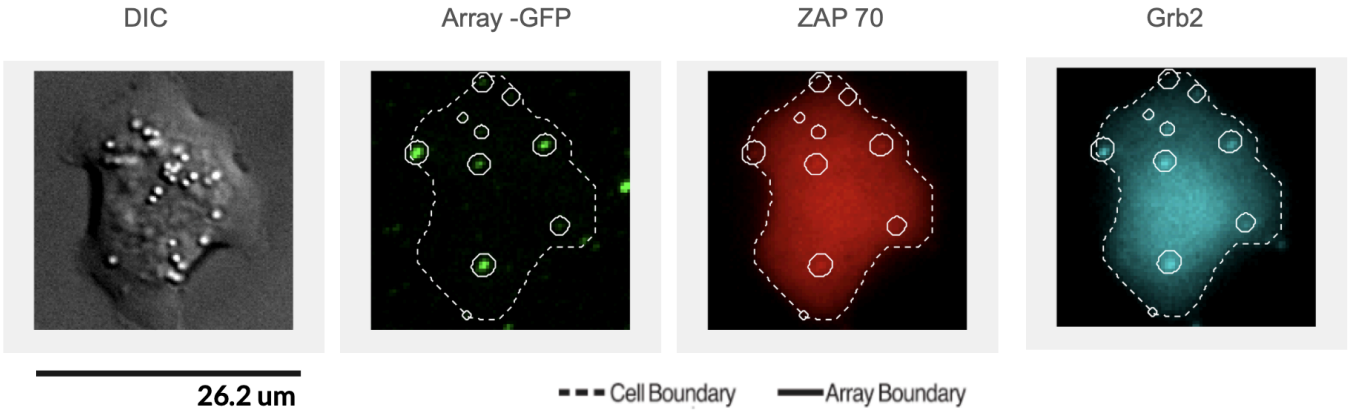

Figure 10: *shows four different channels, including the DIC channel and other channels showing pMHC-GFP arrays, along with ZAP70-XFP and Grb2. The solid circle indicates array locations, and the dashed line is the border of the cell.*

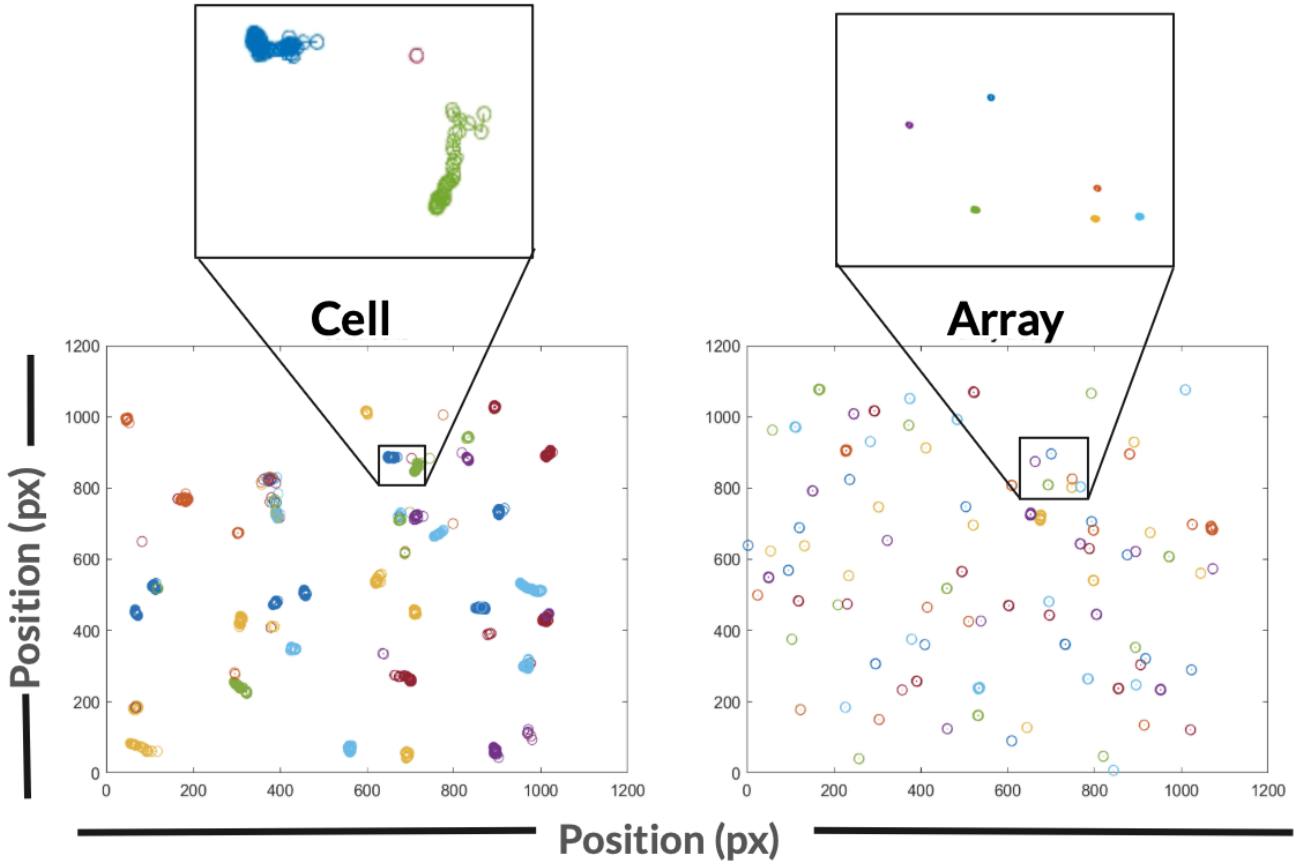

Figure 11: This figure is zoomed in to demonstrate that cells move while arrays do not.*The cell track (left) and the array track(right) over 121 time points of live imaging.*

Additionally, throughout 121 time points, we were able to locate the cell. We monitored the cell from the moment it initially touched the plate's bottom until the very final moment, at which point we noted the period it was likely to hit arrays coated in the plate. The time the cell reached the bottom of the glass plate and made contact with the array was when clustering of Grb2 was activated.

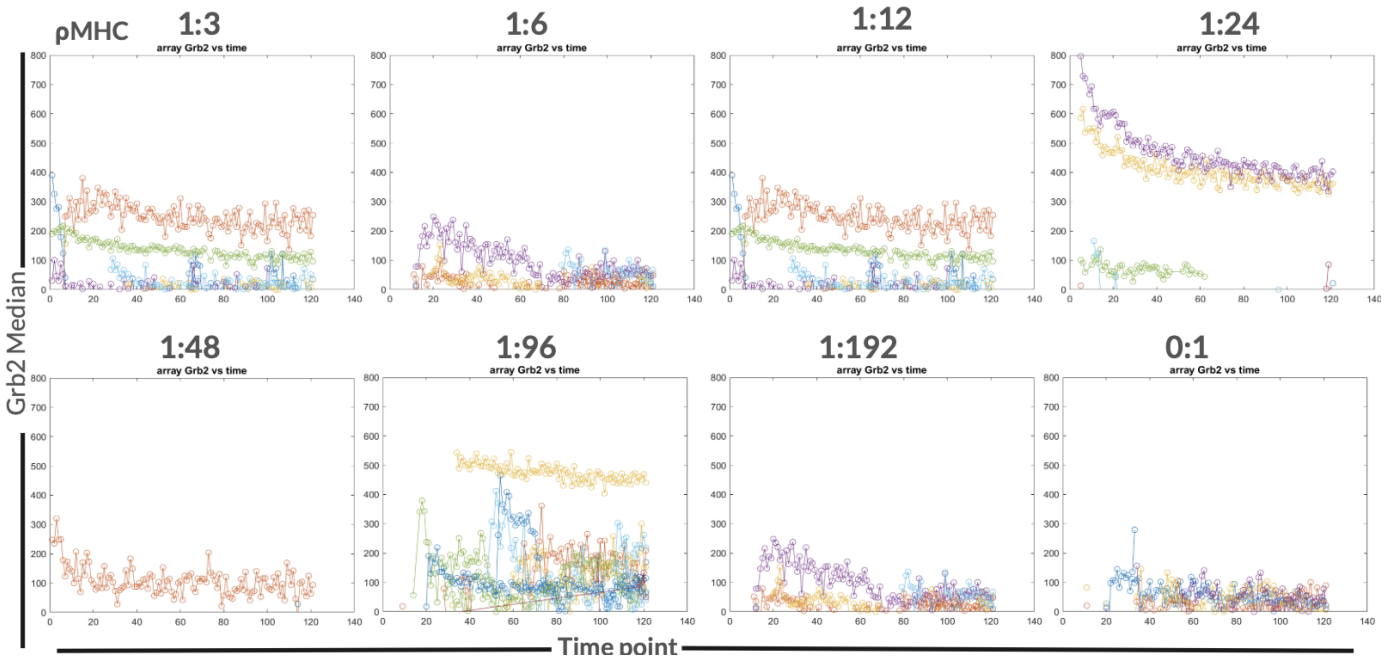

Figure 12 The Grb2 expression is higher in the intermediate pMCH density*. The intermediate (300* pMHC/um^2 *ratio) pMHC has relatively low Grb2 expression on both ends of high and low density.*

The 300 pMHC/um^2 ratio showed the highest Grb2 expressions, with the highest point around 800. The high and low pMHC ratios were less than the highest point of the 1:24 ratio, supporting the model developed by Will White. This behavior was expected, as the intermediate density of pMHC was preferred for T-cell activation, and the 1:24 ratio was the intermediate spacing for pMHC density. The data provided is preliminary and further experiments are required to confirm the results, but suggests that we are able to observe similar effects with live imaging as with fixed cell imaging.

Discussion

The overall goal of this live imaging project is to further study the model that had been developed in our lab. The model predicts an optimal pMHC spacing for T-cell activation, which is consistent with experimental results[3]. The model suggests an intermediate spacing is optimal for LAT cluster formation and T-cell signaling. Simulations showed that pMHC spacing affects pLAT activation efficiency showing a peak at intermediate pMHC spacing[3]. The findings also show that LAT condensation sets the spatial scales of TCR activation in addition to the temporal scales. Thus, LAT condensation plays a crucial role in determining the optimal pMHC spacing for T cell activation, indicating that LAT condensation plays a crucial role in T cell activation.

The kinetics of LAT phosphorylation, diffusion, and condensation following TCR-pMHC binding are examined in the model to understand the function of LAT condensation in TCR signaling. It demonstrates how selective reactions to high-affinity pMHC ligands are made possible by temporal lags in LAT

condensate nucleation[3,7,20]. Additionally, the model shows that cooperativity in LAT condensate nucleation and development grows with increasing antigen numbers and amplifies weak signals from single foreign peptides. The model indicates that nucleation-condensation proofreading is essential for the TCR signaling pathway's antigen detection capacities since it predicts a reliance of signal intensity on pMHC spacing. Live imaging is a valuable method for real-time observation of signaling dynamics, making it an excellent tool for understanding signaling dynamics.

Methods

Cloning reporters

We used TCR, LAT, ZAP, Grb2, and PLCg proteins as markers for T-cell activation and essential for tracking and labeling receptor proteins using mRuby and iRFP. The plasmids used in the cloning procedure include Emerald-PLC, Grb2-Emerald, LAT, TCRzeta, Zap70, and pLenti-EF1a-TPRv2-Asc1. These plasmids are essential for tracking and labeling specific receptor proteins. We retrieved the DNA from those plasmids containing fluorescent proteins using Gibson assembly and transformed them using a Petri dish covered with antibiotics. The essential colonies were grown selectively with the help of two antibiotics, carbenicillin and kanamycin. Three colonies were chosen for each culture, and we ran a PCR on each one before submitting it to Plasmid-Sources for sequencing. After the sequences were sequenced and sent back to us, we aligned them to make sure each reporter we selected had the right sequence and did not contain mutations.

Viral Production

To make the viral production we used the HEK cells. The thawing process of HEK 293T cells involves several steps, including thawing at 37C, dilution, resuspending, washing, incubation, counting, and resuspending in different media and PSG before being transferred to a 6-well plate. The next day, the cells are checked for confluency, and if it is less than 30%, they are waited longer or re-plated. With pMDg2 equal to 2. g 0.311, pMDLg/pRRE equal to 0.476, and pRSV/Rev equal to 0.222 plasmid was calculated and transferred to the 4.5uL fugene. The OptiMEM is aliquoted for 200uL total, and the mixture is then added to the HEK cells. The cells are then incubated for 15 minutes at room temperature. The cells are then returned to the incubator for approximately 16 hours. 24 hours later the extraction of the viral supernatant from the HEK cells. The supernatant is then filtered through a 0.45um filter and aliquoted. The aliquots can be used fresh or frozen for later use.

Viral infection

On the first day, pre-heat a centrifuge to 32C, and add dilute10ug/mL polybrene to the viral supernatant. Mix equal volumes of 1M/mL target cells and viral supernatant. Transfer the virus/cell mixture to a 24-well plate and spin at 2000xg for 1 hour at 32C. Cover the plate in a plastic bag and tape it shut to prevent virus leakage. Return the plate to the incubator overnight. On the second day, mix infected cells and count their numbers. Resuspend cells in fresh TCM to a final density of 100k/mL and plate them in appropriate plate sizes. Incubate at 37C for at least 3 additional days before use or sorting. If incubating for more than 3 days, ensure cells grow at most 1M/mL. On the fifth day, cells are ready to use or freeze.

Sorting

Sorting is a method to distinguish cells that are tagged with fluorescent proteins using a sorting device. The process involved harvesting cells, filtering, staining with fluorescent antibodies, cleaning and washing cells, setting up a flow cytometer, and sorting cells into tubes. In this project, we made six different cell lines by using the viral transfection method. The process involved sorting infected cells, resuspending them in 1mL HBH, and using fewer cells for uninfected control. The cells were collected in 5mL tubes with 1mL of TCM and stored on ice. Two double-positive populations per cell line were collected, and the sorted cells were resuspended in 200uL TCM to grow overnight in 96-well plates. Finally, we analyzed sorted cell data using flowJo to assess purity and viability.

T-Cell Flow Cytometry

The process involves transferring cells to a round-bottom 96-well plate, aspirating media, and re-suspending them in an FC-blocking buffer. The plate should have 50k cells per well. Staining antibodies for cell surface targets are added to the Fc block, and the cells are incubated for 15 minutes at 4 °C. Cells are washed twice with the Fc block, and then resuspended in 150 uL/well FACS buffer and run on the FACS machine.

T-Cell culture

William White provided P14 TCR transgenic Jurkat cells with different stages of cloning and sister clones from each batch, which were cultured in 87% RPMI supplemented with 10% FBS, 1% HEPES, 1% sodium pyruvate, and 1% PSG (Pen, Strep, and Glu). The cells were kept in liquid nitrogen in 500-uL aliquots at 5 million/mL in a T-cell medium with 5% DMSO. The cells were frozen, thawed, transferred, and cultured for two days at 37 °C and 5% CO2 four days before imaging [3]. After two days, they were diluted to 100 k cells/mL in a T-cell medium and incubated for an additional two days at 37 °C and 5% CO2 [3].

Plate coating

The plate was coated with a 100x dilution of anti-GFP antibody, 10ng/uL anti-LFA (CD11a), and 20ng/uL Retronectin, and the cells were incubated at 4C overnight[3]. The protocol involved using an array mix of 1:3, 1:6, 1:12, 1:24, 1:48, 1:96, 1:192, and 1:0 MHC rations.

Fixed imaging

The cells are then fixed in an Fc block, and the staining antibody is mixed with the appropriate volume of each antibody. The cells are then incubated at 4C overnight [3]. The next day, the cells are incubated with BD Cytofix buffer, CTV stock, and CTV dilution. The CTV is then incubated at RT for 20 minutes. The microscope is set up, and the plate is moved to the microscope. The focus is adjusted until the cells are in focus. The autofocus offset is determined, and the live channel is switched to the arrays. The live camera is turned off, and the z-positions are recorded in a spreadsheet. The position file script is run with the new z-positions and autofocus offset, and the final positions are set. The images are then acquired. Images of both fixed and labeled cells were obtained with a Leica DMi8 equipped with a 63x (0.75 NA) glycerol objective, hardware autofocus, and a spinning disc confocal. At every position, a z-stack of six slices was created, with each slice centered on the glass surface and spaced by 200 nm. Images of cells (DIC, 100 ms exposure), CellTrace (405 Ex, 440/40 Em, 500 ms exposure), arrays/GFP (470 Ex; 510/50 Em, 900 ms exposure), PE-anti-pLAT (555 Ex, 600/50 Em, 200 ms exposure), and AF647-anti-pCD3ζ (640 Ex, 700/75 Em, 900 ms exposure) were taken at each slice using an LDI-7 at 50% power[3].

Live imaging

Live imaging is performed similarly to fixed cell imaging, with a few adjustments except we add the 200 uL of the cell at the imaging point rather than adding the cell early to get fixed. We pipette the cells into each well, and the cells slowly fall to the bottom of the well. It takes roughly 3 minutes for most of the cells to touch the bottom of the plate, where the array is present. Using this slow falling of the cell as an advantage, we were able to image cells at the bottom of the plates and arrays up to 121-time points per well and condition. Since we are trying to image them live, we want the cell to freely move around until it reaches the bottom of the plate and touches the array. The arrays were diluted to 50 nM in array buffer and added to each well. T-cell was stained with CTV in 1000 fold with the PBS resuspended cell, then incubated with checking at room temperature for 15 minutes. The FC block was added and resuspended in TCM. The cells were then diluted to 2 million/mL in TCM before being added to the plate. The plate was set to autofocus, and 200 uL of cells were added. The imaging was started to observe early time points, as soon as possible after adding cells. The protocol also included a vibration box and a wide field without confocal imaging. Configuring a microscope retained 5 channels are utilized, using a 63x glycerol objective lens and a 5s imaging period. The channels are DIC. 30-millisecond exposure 405nm laser, 5% power 30-millisecond exposure 470nm laser, 25% power 60-millisecond exposure 555nm laser, 2% power 40-millisecond exposure 640nm laser, 25% power 40-millisecond exposure

Image analysis

The MATLAB program was used to examine the acquired images. Following the acquisition of the images, we loaded the image file into MATLAB, prepared the segmentation of the cells and arrays, and distinguished between good and bad segmentation. We might rerun the segmentation if it turned out to be unsatisfactory by modifying the segmentation parameter. We then verified by going over most of the cell and array segmentation again using the MATLAB code we wrote. If the segmentation looks good, start using the data generated after the segmentation to make plots and analyze them. We extracted data on CD3ζ and LAT phosphorylation in regions where cells interacted with pMHC arrays using a customized MATLAB script. The CellTrace dye was used to segment the cells, identifying areas of the cells. The array and the cell were segmented using this unique MATLAB script. The array and also the cell were traced through all time points. We also analyze when the cell touches the bottom of the pallet and comes into contact with the array.

Flow Cytometry Analysis

To analyze the flow cytometry data we used a software called Flowjo.

References

1. Padhan K, Varma R. Immunological synapse: a multi-protein signaling cellular apparatus for controlling gene expression. *Immunology* 2010;**129**:322–8. https://doi.org/10.1111/j.1365-2567.2009.03241.x.
2. Sanchez E, Huse M. Spatial and Temporal Control of T Cell Activation Using a Photoactivatable Agonist. *Journal of Visualized Experiments* 2018. https://doi.org/10.3791/56655.
3. https://www.biorxiv.org/content/10.1101/2024.03.13.584745v1
4. Charles A Janeway J, Travers P, Walport M, Shlomchik MJ. General properties of armed effector T cells. *Immunobiology: The Immune System in Health and Disease 5th Edition* 2001.
5. Courtney AH, Lo W-L, Weiss A. TCR Signaling: Mechanisms of Initiation and Propagation. *Trends in Biochemical Sciences* 2018;**43**:108–23. https://doi.org/10.1016/j.tibs.2017.11.008.
6. Dustin ML, Chakraborty AK, Shaw AS. Understanding the Structure and Function of the Immunological Synapse. *Cold Spring Harbor Perspectives in Biology* 2010;**2**:a002311–1. https://doi.org/10.1101/cshperspect.a002311.
7. Brownlie RJ, Zamoyska R. T cell receptor signalling networks: branched, diversified and bounded. *Nature Reviews Immunology* 2013;**13**:257–69. https://doi.org/10.1038/nri3403.
8. Lever M, Lim H-S, Philipp Krüger, Nguyen J, Trendel N, Enas Abu-Shah, *et al.* Architecture of a minimal signaling pathway explains the T-cell response to a 1 million-fold variation in antigen affinity and dose. *Proceedings of the National Academy of Sciences of the United States of America* 2016;**113**: https://doi.org/10.1073/pnas.1608820113.
9. Lo W-L, Kuhlmann M, Rizzuto G, Ekiz HA, Kolawole EM, Revelo MP, *et al.* A single-amino acid substitution in the adaptor LAT accelerates TCR proofreading kinetics and alters T-cell selection, maintenance and function. *Nature Immunology* 2023;**24**:676–89. https://doi.org/10.1038/s41590-023-01444-x.
10. Shah N, Wang Q, Yan Q, Deepti Karandur, Kadlecek TA, Fallahee IR, *et al.* An electrostatic selection mechanism controls sequential kinase signaling downstream of the T cell receptor 2016;**5**: https://doi.org/10.7554/elife.20105.
11. Zeng L, Palaia I, Šarić A, Su X. PLCγ1 promotes phase separation of T cell signaling components. *Journal of Cell Biology* 2021;**220**: https://doi.org/10.1083/jcb.202009154.
12. Yi J, Lakshmi Balagopalan, Nguyen T, McIntire KM, Samelson LE. TCR microclusters form spatially segregated domains and sequentially assemble in calcium-dependent kinetic steps. *Nature Communications* 2019;**10**: https://doi.org/10.1038/s41467-018-08064-2.
13. Britain DM, Town JP, Orion David Weiner. Progressive enhancement of kinetic proofreading in T cell antigen discrimination from receptor activation to DAG generation. *ELife* 2022;**11**: https://doi.org/10.7554/elife.75263.
14. Wither MJ, White WL, Pendyala S, Leanza PJ, Fowler DM, Kueh HY. Antigen perception in T cells by long-term Erk and NFAT signaling dynamics. *Proceedings of the National Academy of Sciences of the United States of America*2023;**120**:e2308366120. https://doi.org/10.1073/pnas.2308366120.
15. François P, Voisinne G, Siggia ED, Altan-Bonnet G, Vergassola M. Phenotypic model for early T-cell activation displaying sensitivity, specificity, and antagonism. *Proceedings of the National Academy of Sciences of the United States of America* 2013;**110**:E888-897. https://doi.org/10.1073/pnas.1300752110.

16. Lin J, Low-Nam ST, Alfieri KN, McAffee D, Fay NC, Groves JT. Mapping the stochastic sequence of individual ligand-receptor binding events to cellular activation: T cells act on the rare events. *Science Signaling* 2019;**12**: https://doi.org/10.1126/scisignal.aat8715.
17. Kirby D, Zilman A. Proofreading does not result in more reliable ligand discrimination in receptor signaling due to its inherent stochasticity. *Proceedings of the National Academy of Sciences of the United States of America*2023;**120**:e2212795120. https://doi.org/10.1073/pnas.2212795120.
18. Su X, Ditlev JA, Hui E, Xing W, Banjade S, Okrut J, *et al.* Phase separation of signaling molecules promotes T cell receptor signal transduction. *Science* 2016;**352**:595–9. https://doi.org/10.1126/science.aad9964.
19. Tischer DK, Weiner OD. Light-based tuning of ligand half-life supports kinetic proofreading model of T cell signaling. *ELife* 2019;**8**:e42498. https://doi.org/10.7554/eLife.42498.
20. Zhang W-G, Trible RP, Zhu M, Liu SK, C. Jane McGlade, Samelson LE. Association of Grb2, Gads, and Phospholipase C-γ1 with Phosphorylated LAT Tyrosine Residues 2000;**275**:23355–61. https://doi.org/10.1074/jbc.m000404200.
21. Huang W, Alvarez S, Kondo Y, Young Kwang Lee, Chung JK, Hiu, *et al.* A molecular assembly phase transition and kinetic proofreading modulate Ras activation by SOS. *Science* 2019;**363**:1098–103. https://doi.org/10.1126/science.aau5721.
22. Ganti RS, Lo W-L, McAffee DB, Groves JT, Weiss A, Chakraborty AK. How the T cell signaling network processes information to discriminate between self and agonist ligands. *Proceedings of the National Academy of Sciences of the United States of America* 2020;**117**:26020–30. https://doi.org/10.1073/pnas.2008303117.
23. Tomasz Lipniacki, Hat B, Faeder JR, Hlavacek WS. Stochastic effects and bistability in T cell receptor signaling 2008;**254**:110–22. https://doi.org/10.1016/j.jtbi.2008.05.001.
24. Das J, Ho M, Zikherman J, Govern C, Yang M, Weiss A, *et al.* Digital Signaling and Hysteresis Characterize Ras Activation in Lymphoid Cells. *Cell* 2009;**136**:337–51. https://doi.org/10.1016/j.cell.2008.11.051.
25. McAffee DB, O'Dair MK, Lin JJ, Low-Nam ST, Wilhelm KB, Kim S, *et al.* Discrete LAT condensates encode antigen information from single pMHC:TCR binding events. *Nature Communications* 2022;**13**:7446. https://doi.org/10.1038/s41467-022-35093-9.
26. Sun S, GrandPre T, Limmer DT, Groves JT. Kinetic frustration by limited bond availability controls the LAT protein condensation phase transition on membranes. *Science Advances* 2022;**8**: https://doi.org/10.1126/sciadv.abo5295.
27. Ben-Sasson AJ, Watson JL, Sheffler W, Johnson MC, Bittleston A, Somasundaram L, *et al.* Design of biologically active binary protein 2D materials. *Nature* 2021;**589**:468–73. https://doi.org/10.1038/s41586-020-03120-
28. Lo W-L, Shah NH, Rubin SA, Zhang W, Horkova V, Fallahee IR, *et al.* Slow phosphorylation of a tyrosine residue in LAT optimizes T cell ligand discrimination. *Nature Immunology* 2019;**20**:1481–93. https://doi.org/10.1038/s41590-019-0502-2.
29. Rodríguez-Fernández JL, Criado-García O. The Actin Cytoskeleton at the Immunological Synapse of Dendritic Cells. *Frontiers in Cell and Developmental Biology* 2021;**9**: https://doi.org/10.3389/fcell.2021.679500.
30. Su Q, Mehta S, Zhang J. Liquid-liquid phase separation: Orchestrating cell signaling through time and space. *Molecular Cell* 2021;**81**:4137–46. https://doi.org/10.1016/j.molcel.2021.09.010.

31. Fooksman DR, Vardhana S, Vasiliver-Shamis G, Liese J, Blair DA, Waite J, *et al.* Functional Anatomy of T Cell Activation and Synapse Formation. *Annual Review of Immunology* 2010;**28**:79–105. https://doi.org/10.1146/annurev-immunol-030409-101308.
32. Ni Q, Mehta S, Zhang J. Live‐cell imaging of cell signaling using genetically encoded fluorescent reporters. *The FEBS Journal* 2017;**285**:203–19. https://doi.org/10.1111/febs.14134.
33. https://www.researchgate.net/figure/Phase-separation-in-TCR-signaling-Upon-TCR-activation-LAT-phase-separates-into-a_fig2_363425042
34. Yi J, Lakshmi Balagopalan, Nguyen T, McIntire KM, Samelson LE. TCR microclusters form spatially segregated domains and sequentially assemble in calcium-dependent kinetic steps. *Nature Communications* 2019;**10**: https://doi.org/10.1038/s41467-018-08064-2.
35. Kushnarova-Vakal A, Äärelä A, Huovinen T, Virta P, Lamminmäki U. Site-Specific Linking of an Oligonucleotide to Mono- and Bivalent Recombinant Antibodies with SpyCatcher-SpyTag System for Immuno-PCR. *ACS Omega*2020;**5**:24927–34. https://doi.org/10.1021/acsomega.0c03750.